Design of Multi-permeability Distributed Air-gap Inductors

Laili Wang Zhiyuan Hu Yan-fei Liu
Department of Electrical and Computer Engineering
Queen's University
Kingston, ON, Canada
l.l.wang@queensu.ca

Yunqing Pei Xu Yang
Department of Electrical Engineering
Xi'an Jiaotong University
Xi'an , China
peiyq@mail.xjtu.edu.cn

Abstract— **Distributed air-gap inductors have the advantage of low fringing effect loss. However, the flux density uniformly distributes in the magnetic cores, which results in the magnetic material closer to conductor becoming saturated while the magnetic material far away from the conductor is still not fully utilized. This paper proposes a multi-permeability distributed air-gap inductor structure to increase inductance without the necessity of increasing the inductor volume. The discrete permeability values are investigated. Inductance variations versus number of permeability layers are obtained under the condition that the inductor thickness is constant. To evaluate the proposed method, a three-permeability inductor together with a single permeability inductor is fabricated. The measured results show that the three-permeability inductor has much higher inductance than the single-permeability inductor for the whole load range. Both inductors are tested in a 5V input, 3V output DC/DC converter to compare their performances. The results show the three-permeability inductor could further improve light load efficiency of high frequency DC/DC converters.**

I. INTRODUCTION

The design of inductors used in high frequency DC/DC converters has been very popular in recent years because it plays an important role in increasing the power density and in improving the efficiency. In conventional high frequency DC/DC converters, the inductors are usually constructed with high permeability commercial magnetic cores and copper wires. For these inductors, air-gaps are needed to guarantee the magnetic cores do not become saturated at full load. However, the leakage flux from the air-gap also causes high winding loss, resulting in a reduction of the efficiency [1]. With the purpose of reducing winding loss caused by the air-gap, quasi-distributed air-gap [2-5] and distributed air-gap [6-20] techniques have been proposed. A quasi-distributed air-gap inductor is modified from an air-gap inductor by dividing a large air-gap into some small gaps so that the fringing effect loss could be reduced. To further reduce the fringing effect loss, the distributed air-gap inductors, which is essentially equivalent to dividing the air-gap into finite number of small gaps, have also been proposed [8-25]. However, there is still a problem for designing such a distributed air-gap inductor since it has the disadvantage of nonuniform flux density distribution in the magnetic cores. For air-gaped inductors designed with commercial magnetic cores, the flux density in the core can be seen as uniform, but for distributed air-gap magnetic cores, the flux density in the magnetic cores can no longer be seen as uniform. It varies according to equivalent magnetic reluctance along the flux path. This inevitably leads to insufficient utilization of magnetic material. Fig. 1 roughly illustrates the flux density distributions in three planar magnetic cores with the increase of current. The first magnetic core is made with lower permeability magnetic material, and the second one is made with higher permeability magnetic material. The cross-sections of the both magnetic cores are roughly divided into three regions. Region I has the smallest magnetic reluctance, and Region III has the highest, the Region II's magnetic reluctance is between them. For the first magnetic core, at full load, Region I has high flux density, region II has medium flux density, region III has low flux density. However, at light load, Region II and Region III have very low flux density which means the magnetic material is not fully utilized. For the second magnetic core, at light and medium load conditions, the flux density of Region II and Region III is higher than that of the first magnetic core. However, at full load, Region I becomes saturated. It can be seen that both the first magnetic core and the second magnetic core could not be utilized effectively, especially at light load condition.

This paper proposes to improve the flux density distribution in the magnetic core by gradually increasing the permeability from magnetic material closer to the conductor to further away from the conductor (Region I to Region III as shown in Fig. 1). The improved flux density distribution shown in the third magnetic core is much more uniform.

978-1-4673-0803-8/12/$31.00 ©2012 IEEE

Section II of this paper describes the principle of multi-permeability inductors. Section III analyzes and optimizes the design of multi-permeability distributed air-gap inductors using computer simulation. Section IV presents the experimental results of a three-permeability inductor as well as a single permeability inductor. Characteristics of the inductor prototypes are measured, and the inductors are evaluated in a DC/DC converter for comparison. Section V is the conclusion.

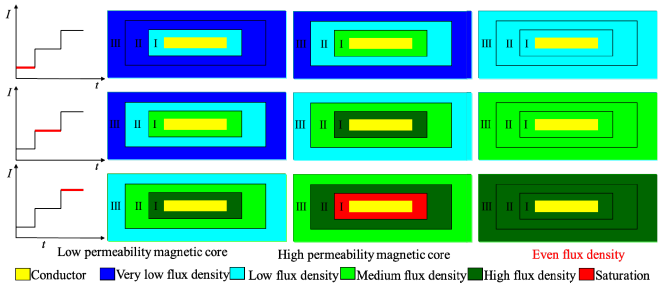

Fig. 1. Flux density distribution in a single permeability inductor.

II. Basic Idea of Multi-permeability Inductor

This section introduces the basic idea and advantages of the multi-permeability distributed air-gap inductors. Two typical kinds of distributed air-gap inductors are analyzed in this paper. One is toroidal inductors with circular cross-section; the other one is planar inductors with square cross-section. For the purpose of simplicity, this paper focuses on one turn inductors based on which multiple turns inductors could be designed. Fig. 2 shows the structures of the inductors. Their cross-sections are shown in Fig. 3. Generally, the flux density in the single permeability magnetic core could be expressed by (1)

$$B_r = \frac{\mu_r \mu_0 I}{l_r} \tag{1}$$

Where l_r is the length of magnetic path, B_r is the corresponding flux density along the path, μ_0 is the permeability of air, μ_r is the relative permeability of the magnetic material.

From the inner surface to the outer surface of the magnetic core, B_r gradually decreases as l_r gradually increases, which causes the uniform distribution of flux density. Fig. 4 shows the flux density distribution of the two magnetic cores under 20A excitation. The nonuniform flux density distribution could be clearly observed. The flux density which is far away from the conductor is still very low while the flux density close to the conductor has reached its peak value B_{max}. This means magnetic material is not fully utilized. The magnetic core could be fully utilized only when flux density at every point of the magnetic core reaches its peak value simultaneously at full load I_f. By increasing the relative permeability of the magnetic material continuously

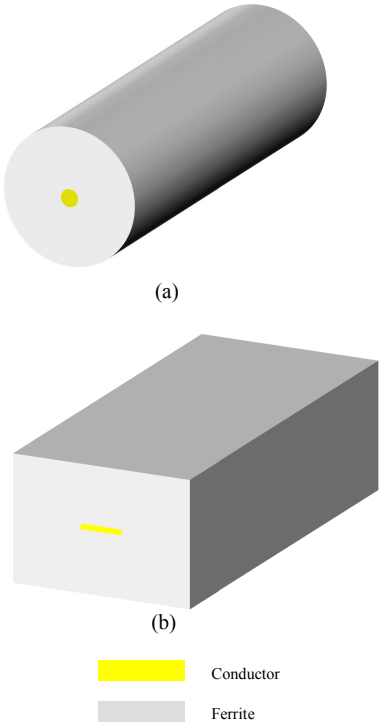

Fig. 2. One turn distributed air-gap inductors. (a) Toroidal inductor. (b) Planar inductor.

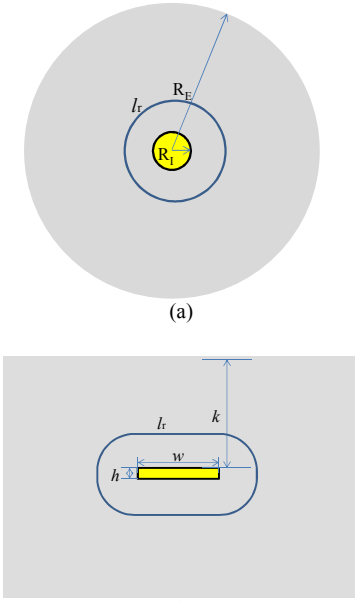

Fig. 3. Cross-section views of single permeability inductors. (a) Circular. (b) Square.

from the inner surface to the outer surface of the magnetic core according to (2), this objective can be achieved. The structures of the continuously changing permeability

magnetic cores are shown in Fig. 5. Based on this way, the magnetic material could be fully utilized and the inductance value could be increased compared with the single permeability inductors.

$$\mu_r(l_r) = \frac{B_{\max} l_r}{\mu_0 I_f} \tag{2}$$

The length of magnetic path for circular cross-section could be expressed by its circumference (3)

$$l_{r\_circular} = 2\pi r \tag{3}$$

Where r is the radius of the circular magnetic path. And the per unit length inductance for a toroidal inductor could be thus expressed by (4)

$$L_{c\_circular} = \int_{R_I}^{R_E} \frac{\mu_r(l_r)\mu_0}{l_{r\_circular}} dr \tag{4}$$

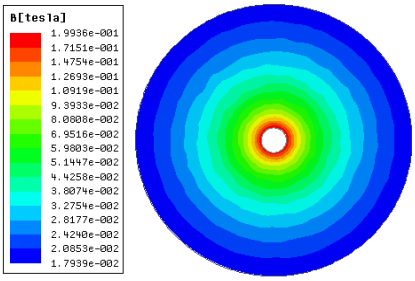

(a)

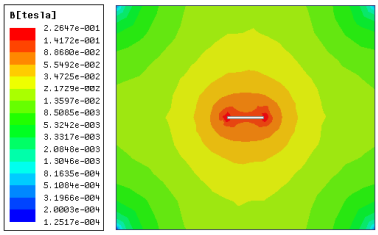

(b)

Fig. 4. Flux density distribution in single permeability distributed air-gap inductors. (a) Circular. (b) Square.

The length of magnetic path of the planar inductors could be expressed by the rectangle. Its length of the magnetic path could be expressed by (5)

$$l_{r\_square} = 2(w+h) + 8k \tag{5}$$

The per unit length inductance for a planar inductor could be expressed by (6)

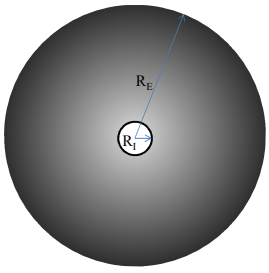

(a)

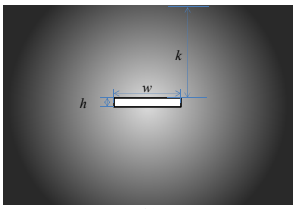

(b)

Fig. 5. Continues changing permeability distribution in distributed air-gap inductors. (a) Circular. (b) Square.

$$L_{c\_square} = \int_0^k \frac{\mu_r(l_r)\mu_0}{l_{r\_square}} dr \tag{6}$$

With such a continuously changing permeability distribution, the whole magnetic core could reach the peak flux density simultaneously, thus the magnetic core is fully utilized. However, it is difficult to fabricate such a continuously changing permeability inductor in practice. Instead, we could divide the region of varying permeability into different small regions, and each small region has a constant permeability. By doing this, a magnetic core whose permeability discretely changes could be realized. The inductors designed with this type of magnetic cores can be called multi-permeability inductors. Fig. 6 shows the structures of magnetic cores with n layers multi-permeability ferrites. Compared with single permeability structure, the proposed magnetic cores have discretely increasing permeability with the increase of radius or height. The permeability expression for toroidal and planar inductors are expressed by (7) and (8)

$$\mu_{ri}(r) = \begin{cases} \mu_{r1} & R_0 \le R < R_1 \\ \cdots & \cdots \\ \mu_{rn-1} & R_{n-2} < R < R_{n-1} \\ \mu_{rn} & R_{n-1} < R < R_n \end{cases} \tag{7}$$

$$\mu_{ki}(r) = \begin{cases} \mu_{s1} & k_0 \le k < k_1 (k_0 = 0) \\ \cdots & \cdots \\ \mu_{sn-1} & k_{n-2} < k < k_{n-1} \\ \mu_{sn} & k_{n-1} < k < k_n \end{cases} \tag{8}$$

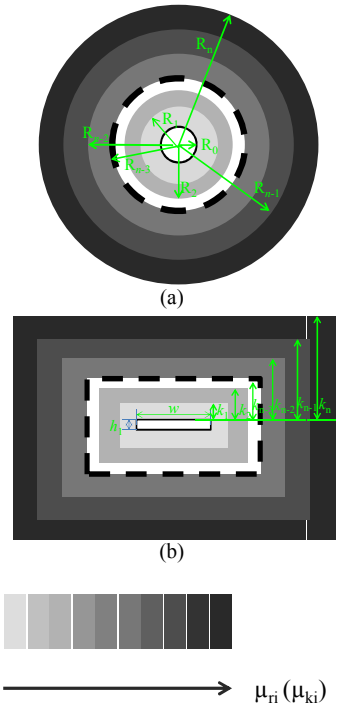

Fig. 6. Discrete permeability distribution in distributed air-gap inductors. (a) Circular. (b) Square.

And the per unit length inductance could be expressed by (9) and (10)

$$L_{d\_circular} = \sum_{i=1}^{n} \int_{R_{i-1}}^{R_i} \frac{\mu_{ri}\mu_0}{l_{r\_circular}} dr \tag{9}$$

$$L_{d\_square} = \sum_{i=1}^{n} \int_{k_{i-1}}^{k_i} \frac{\mu_{si}\mu_0}{l_{r\_square}} dr \tag{10}$$

III. DESIGN OF MULTI-PERMEABILITY INDUCTORS

In this section, four parameters are further analyzed for the optimal design of the toroidal and planar multi-permeability inductors. They are permeability values, the thickness of each permeability layer, number of permeability layers, and radius or height of the inductors. For the simplicity of analysis, three assumptions about the BH curve are made in this section. Fig. 7 shows the assumptive BH curves.

1. The BH curve of each kind of magnetic materials is assumed to be linear before saturation.
2. The permeability becomes μ_0 after saturation.
3. All the magnetic materials have the same peak flux density.

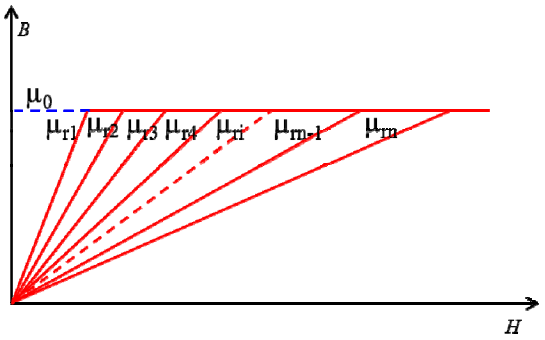

Fig. 7. Realistic BH curve under the assumptions.

A. Permeability distribution

Two three-permeability magnetic cores are taken as examples to illustrate the typical permeability distributions in a multi-permeability inductor. The magnetic cores and their permeability distributions are shown in Fig. 8. The dashed line shows the permeability versus radius for a continuously changing permeability distribution obtained according to (2). As the flux density in (2) is chosen to be the maximum flux density before saturation, permeability obtained through (2) is also the highest permeability at full load. There are three cases for choosing discrete permeability. The first one is discrete permeability is lower than the continuous permeability as in the radius or height range $R<R_1$ ($k<k_1$); the second case is that discrete permeability is higher than one part of continuous permeability, but lower than the other part as in the radius range $R_1<R<R_2$ ($k_1<k<k_2$); The third case is that discrete permeability is completely higher than the continuous permeability as in the range $R_2<R<R_3$ ($k_2<k<k_3$). For the first case, the inductance contributed by this permeability is lower than the continuous permeability distribution, but it will be effective through the whole load range. For the second case, the first part of the magnetic material will become saturated at full load, but the second part is still effective. For the third case, the discrete permeability is completely higher than the continuous permeability, thus its permeability equals to the permeability of air, and has no contribution for total inductance at full load.

An analysis is executed to show the effect of the three typical permeability distributions to inductance values for a specific magnetic material. Fig. 9 shows the three permeability distributions for the magnetic material between R_{i-1} (k_{i-1}) and R_i (k_i). A_0B_0 is the continuous permeability curve between R_{i-1} (k_{i-1}) and R_i (k_{i-1}). A_1B_1 and A_3B_3 show permeability distributions which are lower and higher than the continuous permeability, respectively. A_2B_2 shows the discrete permeability is crossing the continuous permeability curve.

The permeability at A_0 and B_0 could be calculated out for both kinds of inductors. Per unit length inductances versus current will be analyzed separately for the three cases.

For circular shape

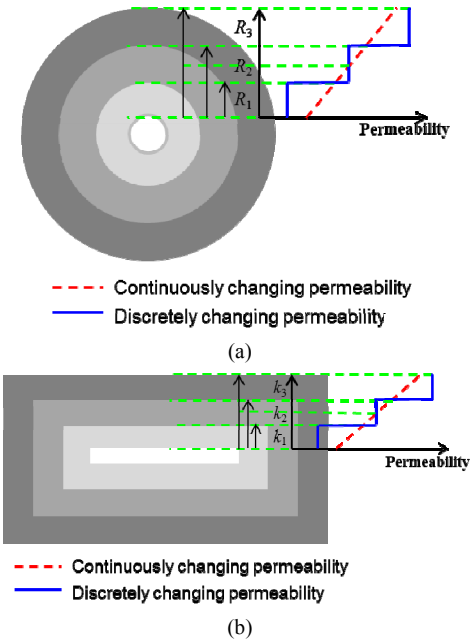

Fig. 8. Two three-permeability inductors and the permeability distributions. (a) Circular. (b) Square.

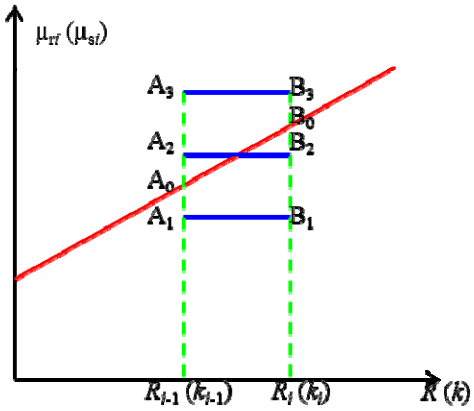

Fig. 9. Three caes of discrete permeability distributions.

$$\mu_r(A_0) = \frac{B_{\max} 2\pi R_{i-1}}{\mu_0 I_f} \tag{11}$$

$$\mu_r(B_0) = \frac{B_{\max} 2\pi R_i}{\mu_0 I_f} \tag{12}$$

For square shape

$$\mu_s(A_0) = \frac{2B_{\max}(w+h+4k_{i-1})}{\mu_0 I_f} \tag{13}$$

$$\mu_s(B_0) = \frac{2B_{\max}(w+h+4k_i)}{\mu_0 I_f} \tag{14}$$

1) The first case (A1B1)

The permeability at point A_1 is lower than the continuous permeability; therefore, the flux density of point A_1 is lower than B_{max} for the whole load range.

2) The second case (A2B2)

The permeability at point A_2 is higher than that at point A_0 while the permeability at point B_2 is still lower than that of point B_0. This means no saturation has occurred as (15) and (16) are satisfied. However, when the current increases further, there's saturation occurs from R_{i-1} (k_{i-1}).

$$I < \frac{\mu_r(A_0)}{\mu_r(A_2)} I_f \tag{15}$$

$$I < \frac{\mu_s(A_0)}{\mu_s(A_2)} I_f \tag{16}$$

3) The third case (A3B3)

The permeability of point A_3 is higher than that of point B_0. Therefore, the inductance calculation can be divided into three stages as the current gradually increases. At first, the inductance of toroidal inductor and the inductance of planar inductor are actually the same with the first case except that the permeability is higher. As the current further increases and (17) and (18) become satisfied, the magnetic materials begin to saturate from the R_{i-1} (k_{i-1}). When the current reaches as high as expressed in (19) and (20), the magnetic core becomes completely saturated, and the inductances are zero.

$$\frac{\mu_r(A_0)}{\mu_r(A_3)} I_f \le I \le \frac{\mu_r(B_0)}{\mu_r(A_3)} I_f \tag{17}$$

$$\frac{\mu_s(A_0)}{\mu_s(A_3)} I_f \le I \le \frac{\mu_s(B_0)}{\mu_s(A_3)} I_f \tag{18}$$

$$I > \frac{\mu_r(B_0)}{\mu_r(A_3)} I_f \tag{19}$$

$$I > \frac{\mu_s(B_0)}{\mu_s(A_3)} I_f \tag{20}$$

Based on the above analysis, the inductances versus current for the three cases are illustrated in Fig. 10. For case one, the inductances keep constant for the whole load range, but it has the lowest inductance at light load. For case two and case three, the permeability is higher, thus the inductances at light load are higher, but they have a drop near the full load. To guarantee the inductance value at full load, the permeability at R_{i-1} (k_{i-1}) should not be higher than

the continuous permeability at Point A_0 which is $\mu_r(A_0)$ or $\mu_s(A_0)$. However, the magnetic material still could not be utilized fully if the permeability is lower than $\mu_r(A_0)$ or $\mu_s(A_0)$ as in the first case. Therefore, to increase the inductance as much as possible, the highest permeability for magnetic material between R_{i-1} (k_{i-1}) and R_i (k_i) is $\mu_r(A_0)$ ($\mu_s(A_0)$).

B. *Number of permeability layers of inductor with constant radius or height*

Previous sub-section derived the optimal permeability value between R_{i-1} and R_i, or between k_{i-1} and k_i with the purpose of obtaining the highest inductance value. Another factor that influences the inductance value is the number of permeability layers in the magnetic core. Multi-permeability structure is essentially an intermediate state between single permeability structure and continuous permeability structure which can be seen as a multi-permeability structure with infinite number of permeability. To illustrate the impact of number of permeability layers on inductance, a calculation is made in this sub-section to show the inductance value versus number of permeability. Fig. 11 shows the discrete inductance values with the number of permeability layers. As the number of permeability layers gradually increases from 1 to 50, the inductance for toroidal inductor increases from 39μH to 59μH (for square cross-section, the inductance increases from 26μH to 70μH). And the inductances become closer and closer to the inductances of the inductors formed with continuously changing permeability magnetic cores. Considering the inductance value gain and complexity of the manufacturing process, it is suggested that 3~10 layers are used for general design.

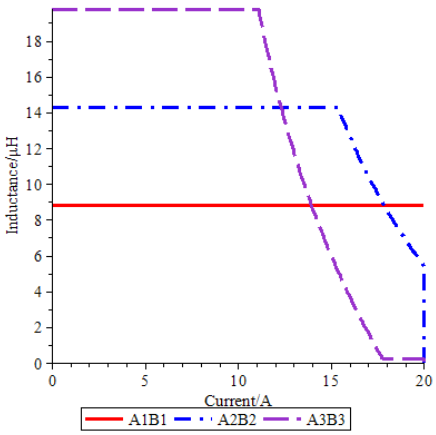

(a)

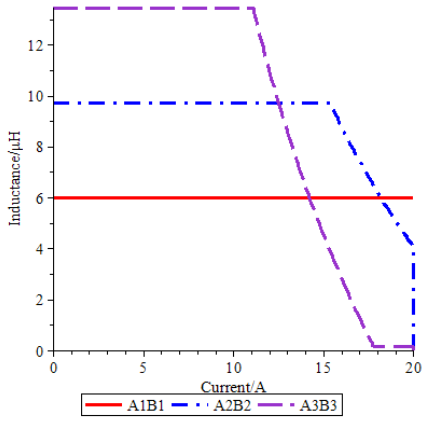

(b)

Fig. 10. Per unit length inductance versus current for different permeability configurations. (a) Circular. (b) Square.

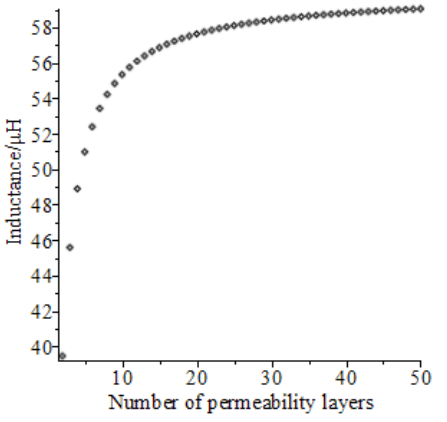

(a)

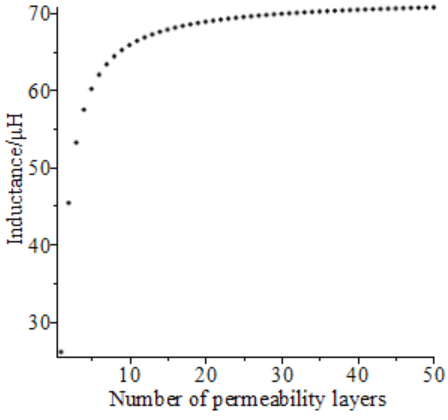

(b)

Fig. 11. Inductance values versus number of permeability. (a) Circular (R_0=1mm, R_n=5mm). (b) Square (w=3mm, h=0.1mm, k_1=0.2mm, k_n=5mm).

IV. Prototype Fabrication and Experiment

To identify inductance increasing effect of the multi-permeability inductors, a three-permeability inductor is fabricated in this section. For the purpose of comparison, a single permeability inductor of the same volume is also fabricated. Their pictures are shown in Fig. 12. The cross section-views are shown in Fig. 13. The windings for both single permeability and three-permeability inductors are copper wires with 1mm radius. Three kinds of the ferrite sheets are selected to make the magnetic cores. They are

C350 from Epcos, IRJ04 and IRJ09 from TDK. They have relative permeability 9, 40 and 100, respectively. The three-permeability inductor is designed by using C305 as the inner layer, IRJ04 as the middle layer, and IRJ09 as the outer layer. Due to the lack of available magnetic sheets with desired permeability, the thickness for each kind of permeability could not be designed to be the same. In order to avoid saturation for each layer, the thicknesses for the three kinds of materials are designed to be 1.5mm, 2mm and 1mm, respectively.

A 5V input 3V output buck converter is constructed to test the two inductor prototypes. The two inductors are firstly applied in the converter to obtain their inductances versus current curve by measuring the peak-peak current ripple. The results are shown in Fig. 14. The single permeability inductor has nearly constant inductance for the whole load range, which is 100nH. For the three-permeability inductor, the light load inductance is 280nH, which is almost three times the single permeability inductor, but it gradually drops to 200nH due to nonlinear characteristic of the BH curve. The efficiencies of the converter with the two inductors are also tested to show the effect of efficiency improvement of multi-permeability inductors for its higher inductance leading to lower current ripple. The results are shown in Fig.15. The efficiency of the converter with the three-permeability inductor is about 5% higher than that with the single permeability, which means the multi-permeability inductor could help to improve the efficiency of the converters.

Fig. 12. Pictures of the inductor prototypes.

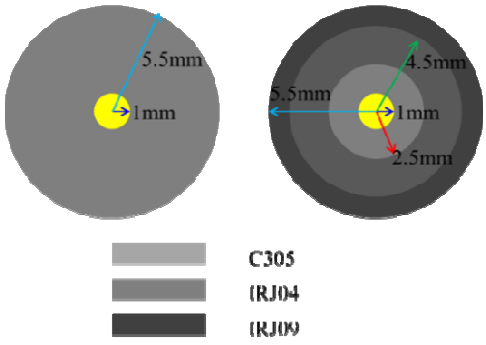

Fig. 13. Cross-section views of the three-permeability inductor and single permeability inductor.

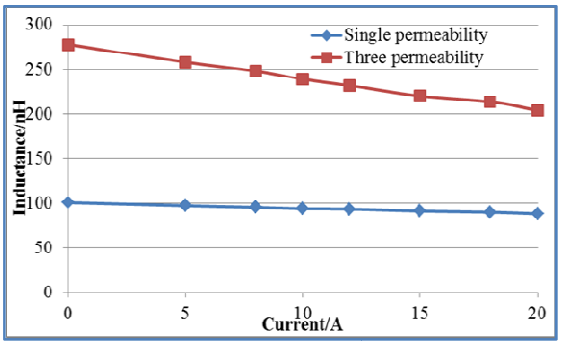

Fig. 14. Inductance versus current.

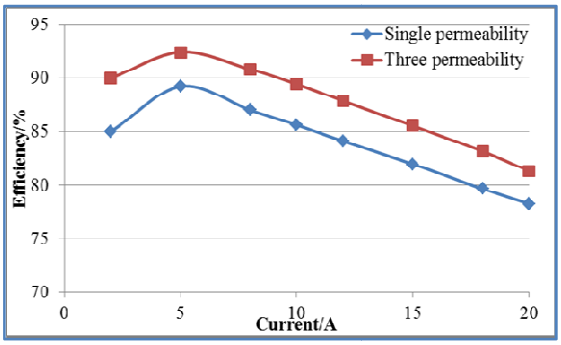

Fig. 15. Efficiency versus current.

V. CONCLUSIONS

This paper proposed multi-permeability inductor structure to improve noruniformly distributed flux density of distributed air-gap inductors. Based on the structure, analysis shows that the inductance value could be significantly increased. Permeability values, number of permeability layers are analyzed to optimize the design of a multi-permeability inductor. The most effective permeability for each layer of ferrites is to make it equal to the corresponding continuous permeability at inner radius or height. Increasing the number of segments could also increase the inductance value, but the effect is less and less significant as the number of segments get larger. To identify the inductance increase effect, a three-permeability inductor and a single permeability inductor of the same volume are made for comparison. The single permeability inductor has nearly constant inductance 100nH for the whole load range while the three-permeability inductor has 280nH inductance at light load and 200nH inductance at full load. Compared with the single permeability inductor, the three-permeability inductor could improve efficiency of a DC/DC converter by 5%.

REFERENCES

[1] Ngo, K. D. T. and M. H. Kuo. "Effects of air gaps on winding loss in high-frequency planar magnetics," in Proc. *IEEE Power Electron. Spec. Conf.*, 1988. Vol.2, pp.1112-1119.

[2] Chew, W. M., Evans, P. D. and Heffernan, W. J. "High frequency inductor design concepts," in Proc. *IEEE Power Electron. Spec. Conf.*, 1991. pp.673-678.

[3] Luca Daniel, Charles R. Sullivan and Seth R. Sanders "Design of microfabricated inductors," *IEEE Trans. Power Electron.*, vol. 14, pp.709-723, Jul. 1999.

[4] Jiankun, H. and C. R. Sullivan. "AC resistance of planar power inductors and the quasidistributed gap technique," *IEEE Trans. Power Electron.*, vol 16, pp.558-567, 2001.

[5] Jianing Wang, Xu Yang, Huapeng Niu, Zhaoan Wang, Jinjun Liu. "PCB integrated transformer composed with ferrite mosaics for LLC resonant converter," in Proc. *IEEE Energy Conversion Congress and Exposition*, 2009. pp.1032-1038.

[6] Qiang, Li, M. Lim, Julu Sun, Arthur Ball, Yucheng Ying, Fred C. Lee, K.D.T. Ngo. "Technology road map for high frequency integrated DC-DC converter." in Proc. *IEEE Applied Power Electronics Conf.*, 2010, pp. 533-539.

[7] Srinivasan Iyengar, Trifon M. Liakopoulos and Chong H. Ahn, "A DC/DC boost converter toward fully on-chip integration using new micromachined planar inductors", in proc. *Power Electronics Specialists Conf.*, 1999, pp. 72-76.

[8] Yasushi Katayama, Satoshi Sugahara, Haruo Nakazawa, Masaharu Edo, "High-Power-Density MHz-Switcing Monolithic DC-DC Converter with Thin-Film Inductor.", in proc. *Power Electronics Specialists Conf.*, 2000, pp. 1485-1490.

[9] Parul Dhagat, Satish Prabhakaran, and Charles R. Sullivan, "Comparison of magnetic materials for V-groove inductors in optimized high-frequency DC-DC converters." *IEEE Trans. Magn.*, vol. 40, no. 4, pp. 2008-2010, July 2004.

[10] Sullivan, C. R. and S . R. Sanders, "Design of microfabricated transformers and inductors for high-frequency power conversion." *IEEE Trans. Power Electron.*, vol. 11, no. 2, pp. 228-238, Mar. 1996.

[11] E. Waffenschmidt, B. Ackermann, J. A. Ferreira, "Design Method and Material Technologies for Passives in Printed Circuit Board Embedded Circuits," *IEEE Trans. Power Electron.*, vol. 20, no. 3, pp. 576-584, May. 2005.

[12] Matthias Ludwig, Maeve Duffy, Terence O'Donnell, Paul McCloskey, and Seán Cian Ó Mathùna, "PCB Integrated Inductors for Low Power DC/DC Converter", *IEEE Trans. Power Electron.*, vol. 18, no. 4, pp. 937-945, July. 2003.

[13] C.-Y. Kim, H.-J. Kim, and J.-R. Kim, "An integrated LTCC inductor," *IEEE Trans. Magn.*, vol. 41, pp. 3556-3558, 2005.

[14] H.-J. Kim, Y.-J. Kim, and J.-R. Kim, "An Integrated LTCC Inductor Embedding NiZn Ferrite," *IEEE Trans. Magn.*, vol. 42, pp. 2840-2842, 2006.

[15] M. H. Lim, J.D. van Wyk, Zhenxian Liang, "Effect of geometry variation of LTCC distributed air-gap filter inductor on light load efficiency of DC-DC converters," in *IEEE Industry Applications Conference*, 2006, pp.1884-1890.

[16] M. H. Lim, Zhenxian Liang, and J. D. van Wyk, "Low Profile Integratable Inductor Fabricated Based on LTCC Technology for Microprocessor Power Delivery Applications," *IEEE Trans. Compon. Packag. Technol.*, vol. 30, pp. 170-177, 2007.

[17] M. H. Lim, J. D. van Wyk, F. C. Lee, and K. D. T. Ngo, "A Class of Ceramic-Based Chip Inductors for Hybrid Integration in Power Supplies," *IEEE Trans. Power Electron.*, vol. 23, pp. 1556-1564, 2008.

[18] M. H. Lim, J. D. van Wyk, and F. C. Lee, "Hybrid Integration of a Low-Voltage, High-Current Power Supply Buck Converter With an LTCC Substrate Inductor," *IEEE Trans. Power Electron.*, vol. 25, pp. 2287-2298, 2010.

[19] Qiang Li, Yan Dong, F. C. Lee. "High density low profile coupled inductor design for integrated Point-of-Load converter," in proc. *IEEE Applied Power Electronics Conference*, 2010, pp.79-85.

[20] Mingkai Mu, Yipeng Su, Qiang Li, F. C. Lee. "Magnetic characterization of low temperature co-fired ceramic (LTCC) ferrite materials for high frequency power converters," in Proc. *IEEE Energy Conversion Congress and Exposition (ECCE)*, 2011, pp.2133-2138.

[21] M. H. Lim, J. D. van Wyk, F. C. Lee. "Hybrid Integration of a Low-Voltage, High-Current Power Supply Buck Converter With an LTCC Substrate Inductor," *IEEE Trans. Power Electron.*, vol. 25, pp.2287-2298, Sep. 2010.

[22] Laili Wang, Yunqing Pei, Xu Yang, Xizhi Cui, and Zhaoan Wang, "Three-dimensional integration of high frequency DC/DC converters based on LTCC technology," in *IEEE Power Electronics and Motion Control Conf.*, 2009., pp. 745-748.

[23] Laili Wang, Yunqing Pei, Xu Yang, Zhaoan Wang, "Design of Ultrathin LTCC Coupled Inductors for Compact DC/DC Converters." *IEEE Trans. Power Electron.*, vol. 26, pp.2528-2541, Sep. 2011.

[24] Laili Wang, Yunqing Pei, Xu Yang, Xizhi Cui, Zhaoan Wang, Guopeng Zhao, "Design of multi-turn LTCC inductors for high frequency DC/DC converters," in proc. *IEEE Applied Power Electronics Conference*, 2010, pp.1610-1615.

[25] Laili Wang, Yunqing Pei, Xu Yang, Qin Yang, and Zhaoan Wang. "Improving Light and Intermediate Load Efficiencies of Buck Converters with Planar Nonlinear Inductors and Variable On Time Control," *IEEE Trans. Power Electron.*, vol. 27, pp. 342-353, Jan. 2012.